Hindawi
Journal of Nanomaterials
Volume 2019, Article ID 6130152, 11 pages
https://doi.org/10.1155/2019/6130152

Research Article

Adsorption of Carbon Dioxide, Methane, and Nitrogen Gases onto ZIF Compounds with Zinc, Cobalt, and Zinc/Cobalt Metal Centers

Ahmed Awadallah-F,[1] Febrian Hillman,[2] Shaheen A. Al-Muhtaseb,[1] and Hae-Kwon Jeong[2,3]

[1]*Department of Chemical Engineering, Qatar University, P.O. Box 2713, Doha, Qatar*
[2]*Artie McFerrin Department of Chemical Engineering, Texas A&M University, College Station, TX 77843-3122, USA*
[3]*Department of Materials Science and Engineering, Texas A&M University, College Station, TX 77843-3122, USA*

Correspondence should be addressed to Shaheen A. Al-Muhtaseb; s.almuhtaseb@qu.edu.qa

Received 14 May 2019; Revised 10 November 2019; Accepted 18 November 2019; Published 23 December 2019

Guest Editor: Fei Ke

ZIF-8, Co-ZIF-8, and Zn/Co-ZIF-8 are utilized in adsorbing nitrogen (N_2), methane (CH_4), and carbon dioxide (CO_2) gases at temperatures between 25 and 55°C and pressures up to ~1 MPa. Equilibrium adsorption isotherms and adsorption kinetics are studied. The dual-site Langmuir equation is employed to correlate the nonisothermal adsorption equilibrium behavior. Generally, N_2 showed the lowest equilibrium adsorption quantity on the three samples, whereas CO_2 showed the highest equilibrium adsorption capacity. Amid the ZIF samples, the biggest adsorption quantities of N_2 and CH_4 were onto Zn/Co-ZIF-8, whereas the highest adsorption quantity of CO_2 was on ZIF-8. The isosteric heats of adsorbing these gases on ZIF-8, Co-ZIF-8, and Zn/Co-ZIF-8 were examined. Moreover, the overall mass transfer coefficients of adsorption at different temperatures were investigated.

1. Introduction

Zeolitic imidazolate frameworks (ZIFs) are convenient substances for gas separation and purification applications. The main reason is their outstanding properties such as excellent chemical and thermal stabilities, surface areas, microporous structures, and synthesis controllability [1, 2]. ZIF-8 possesses a large pore size of 11.6 Å and a small aperture size of 3.4 Å with a zinc metal center linked by an imidazole-type of organic linkers, which looks like a neutral zeolitic sodalite topology [3].

Microwave technology attracted attention in the last decade for the chemical fabrication of nanoporous materials [4, 5]. The microwave-irradiation technique is featured with homogenous and rapid heating with controllable rates [6], which significantly decreases the synthesis time and increases the product yield [7]. To the authors' knowledge, only few works have tackled the subject of the microwave-assisted fabrication of ZIF-8 [8, 9]. The preparation of ZIF-8 products involves several stages of crystal growth, which starts with unstable clusters under super-saturation conditions [10]. Different variables (e.g., heat, diluent vaporization, and molar ratios) influence the product formation in the microwave-assisted preparation process [11].

The climate change phenomenon, which is driven highly by the CO_2 discharge into the atmosphere, draws the concern of the scientific community from different fields. Therefore, the reduction of the anthropogenic CO_2 gas emissions in the atmosphere has become one of the most urgent climate problems to be confronted [12]. Therefore, the improvement of a proficient adsorbent for carbon dioxide gas is a dire need and a necessary step to alleviate this problem [13]. Approximately 30% of CO_2 gas emitted to the atmosphere emerges from fossil-fuel-based power plants and different human life activities [12]. Hence, it is necessary to separate the CO_2 found in flue gases before being exhausted to the atmosphere. Natural gas is known as an alternative and cleaner energy source to replace coal and petroleum. Nonetheless, it involves undesired impurities of CO_2 and N_2, which cause a corrosive impact in pipelines and lower the calorific value of natural gas [14]. Therefore, natural gas requires a pretreatment to remove these impurities before industrial applications [15].

Overall, worldwide research has exerted extreme efforts to develop concise and decisive methods for removing post combustion CO_2 from gas mixtures [16–18]. Methods involving absorption, cryogenic distillation, and physical adsorption are developed to split up carbon dioxide, methane, and nitrogen gas mixtures [19–22].

The aim of this paper is to utilize ZIF compounds, in its virgin shape and after fractional and complete replacement of zinc by cobalt (to form Co-ZIF-8 and Zn/Co-ZIF-8), in order to adsorb CH_4, N_2, and CO_2 gases at four temperatures (ranging from 25 to 55°C) and pressures up to ~1 MPa. The influence of conformational metal content (zinc, cobalt, or zinc/cobalt) of ZIFs on their adsorption behaviors will be studied. The dual-site Langmuir equation will be applied to correlate the adsorption equilibrium data at various temperatures collectively, and the corresponding adsorption isosteric heats of CH_4, N_2, and CO_2 will be estimated. Moreover, the overall mass transfer coefficients for the adsorption of these gases on ZIFs will be examined at various temperatures.

2. Materials and Methods

2.1. Materials. Zinc nitrate hexahydrate (98%, Sigma Aldrich), cobalt nitrate hexahydrate (≥99.99%), and 2-methylimidazole (97%) were purchased from Sigma-Aldrich. Methanol (99.8%) was supplied from Alfa Aesar. Gases (CH_4, N_2, and CO_2) were of high purity (99.999%) and were supplied from the National Industrial Gas Plants (NIGP, Doha, Qatar). All chemical reagents were utilized without further purification.

2.2. ZIF Compound Preparation. Various ZIF compounds (Zn-ZIF (i.e., ZIF-8), Co-ZIF-8, and Zn/Co-ZIF-8) were synthesized by a microwave-assisted method as detailed elsewhere [23].

2.3. Characterization. The characterization results of these ZIFs are found in a previous work [23]. Adsorption equilibrium isotherms of CH_4, N_2, and CO_2 gases were measured via a Hygra magnetic suspension microbalance (MSB, Rubotherm), with microgram sensitivity, following the same procedures described elsewhere [24].

2.4. Theory

2.4.1. Adsorption. The multisite Langmuir model supposes that a heterogeneous surface of an adsorbent is composed of patches with distinctive adsorption energies. Each patch is thus considered as a homogeneous portion of the adsorbent surface, and the total quantity adsorbed of a gas component can be correlated as

$$n_{\text{ads}} = \sum_{j=1}^{J} \frac{m_j b_j P}{1 + b_j P}, \tag{1}$$

where J is the number of homogeneous adsorption patches and it depends on the extent of surface heterogeneity (usually, J is set to 2, corresponding to the dual-site Langmuir (DSL) model), j refers to adsorption patch number, P indicates pressure, m_j refers to the quantity of monolayer saturation on patch j, and b_j indicates the tendency (affinity) for adsorbing the molecules on patch j as estimated by

$$b_j = b_j^0 \exp\left(\frac{\varepsilon_j}{RT}\right), \tag{2}$$

where b_j^0 refers to the adsorption affinity on patch j at infinite temperature, ε_j refers to the characteristic adsorption energy on patch j, R refers to the universal gas constant, and T refers to absolute temperature.

2.4.2. Isosteric Heat of Adsorption. The isosteric heat of adsorption (Q_{st}) can be estimated by the Clausius-Clapeyron approximation [25] as

$$Q_{\text{st}} = -R \left[\frac{\partial lnP}{\partial(1/T)}\right]_n. \tag{3}$$

The dependence of Q_{st} on surface coverage is an implicit indicator of energetic characteristics between the adsorbed molecules and the adsorbent [26].

2.4.3. Adsorption Kinetics. The adsorption rate is determined by the linear driving force (LDF) approximation as [27]

$$\left(\frac{n_t}{n_e}\right) = \left(1 - e^{-kt}\right), \tag{4}$$

where n_t (mole/kg) refers to the adsorbed quantity at time t (sec), n_e (mole/kg) refers to the adsorbed equilibrium quantity at the corresponding temperature and pressure, and k denotes the overall mass transfer coefficient (sec^{-1}). The k-value can be estimated from experimental dynamic adsorption results at a specific temperature and pressure by plotting the $-\ln(1 - n_t/n_e)$ against t until reaching the equilibrium state.

2.4.4. Regression Analysis. Regression was used to obtain the optimum fitting parameters. The least sum of squared errors (LSSE) is widely utilized for regression as [28]

$$\text{LSSE} = \text{Minimum}\left[\sum_{i=1}^{N} \left(n_{i,\text{Calc}} - n_{i,\text{meas}}\right)^2\right], \tag{5}$$

where i indicates measured data point numbers, N denotes the total number of measured data points, and $n_{i,\text{Calc}}$ and $n_{i,\text{meas}}$ refer, respectively, to the calculated and measured quantities adsorbed.

The averaged relative error (ARE, %) was utilized in order to estimate the accuracy of fitting to describe measured data as [29]

$$\text{ARE}\,(\%) = \frac{100\%}{N} \sum_{i=1}^{N} \frac{\left|n_{i,\text{Calc}} - n_{i,\text{meas}}\right|}{n_{i,\text{meas}}}. \tag{6}$$

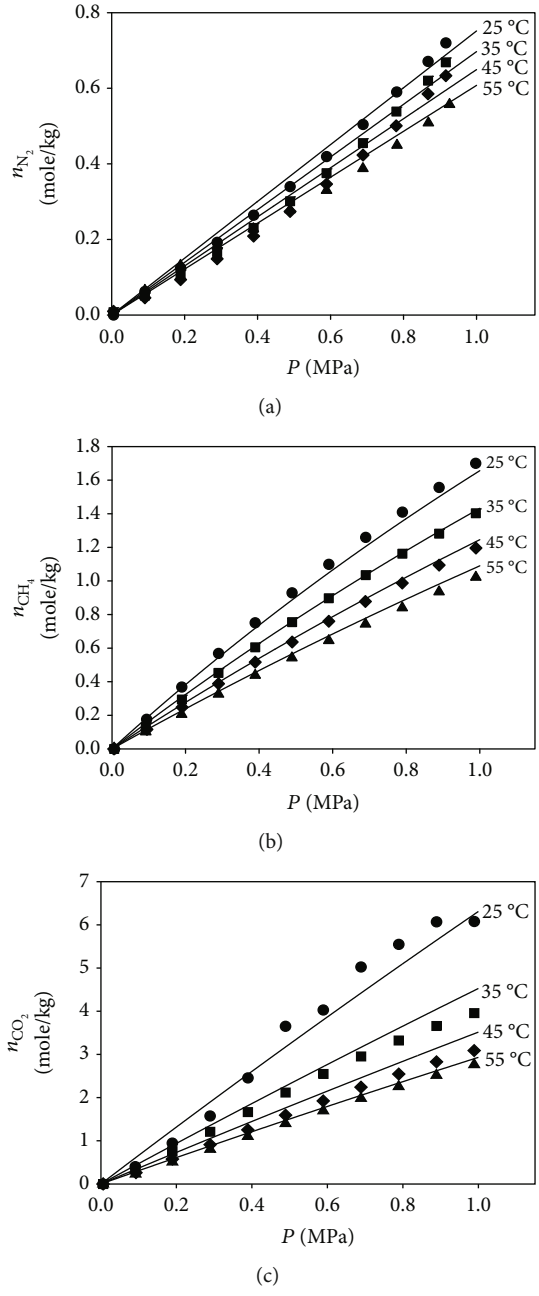

Figure 1: The adsorption equilibria of (a) nitrogen, (b) methane, and (c) carbon dioxide gases on ZIF-8 at different temperatures. The symbols indicate measured results and the lines indicate DSL fitting.

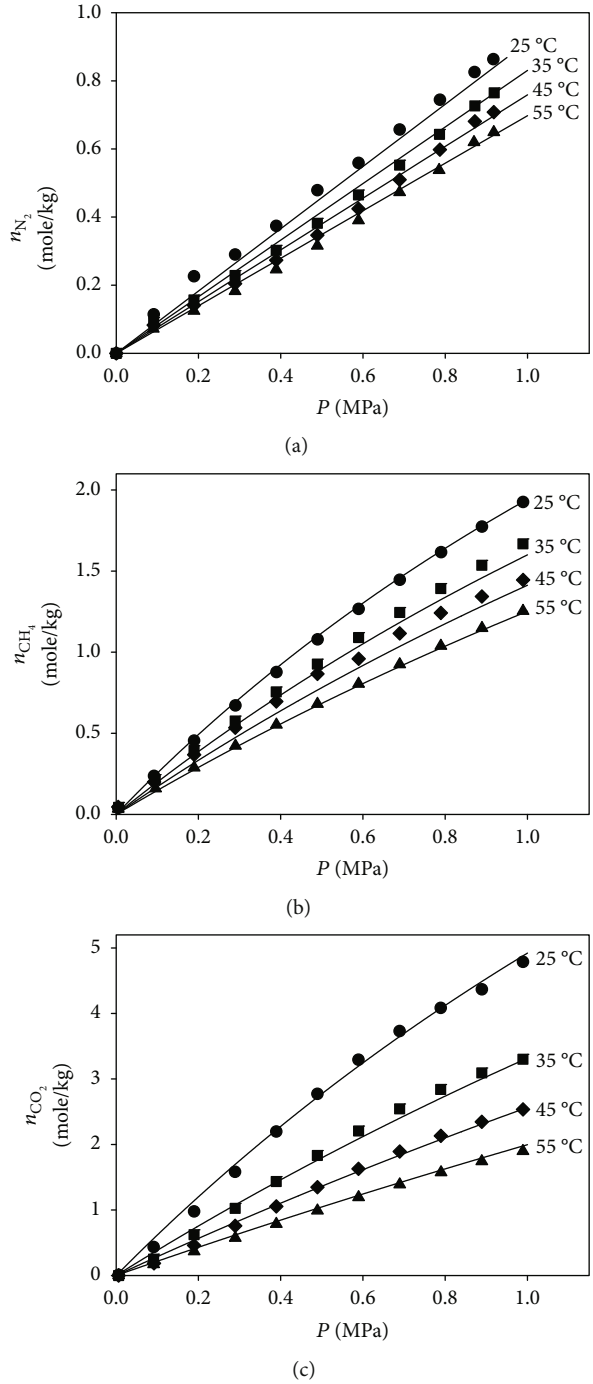

Figure 2: The adsorption equilibria of (a) nitrogen, (b) methane, and (c) carbon dioxide on gases Co-ZIF-8 at different temperatures. The symbols indicate measured results and the lines indicate DSL fitting.

3. Results and Discussion

3.1. Adsorption Equilibrium Isotherms. The adsorption of nitrogen, methane, and carbon dioxide gases onto ZIF-8, Co-ZIF-8, and Zn/Co-ZIF-8 at different temperatures is presented in Figures 1–3, respectively. Broadly, it is seen that the adsorption quantity decreases at higher temperatures. Overall, N_2 gas exposes the lowest adsorbed quantity, whereas CO_2 shows the highest adsorbed quantity. The DSL equation is applied to fit the experimentation results of nitrogen, methane, and carbon dioxide as a function of both temperature and pressure. The fitting parameters registered in Table 1 exposed a good relation with measured results as seen in the solid lines in Figures 1(a)–1(c) to Figures 3(a)–3(c) and by values of ARE (%) in Table 1. Figures 1(a)–1(c) exhibit the adsorption results of nitrogen, methane, and carbon dioxide, respectively, on ZIF-8. It is observed that adsorption

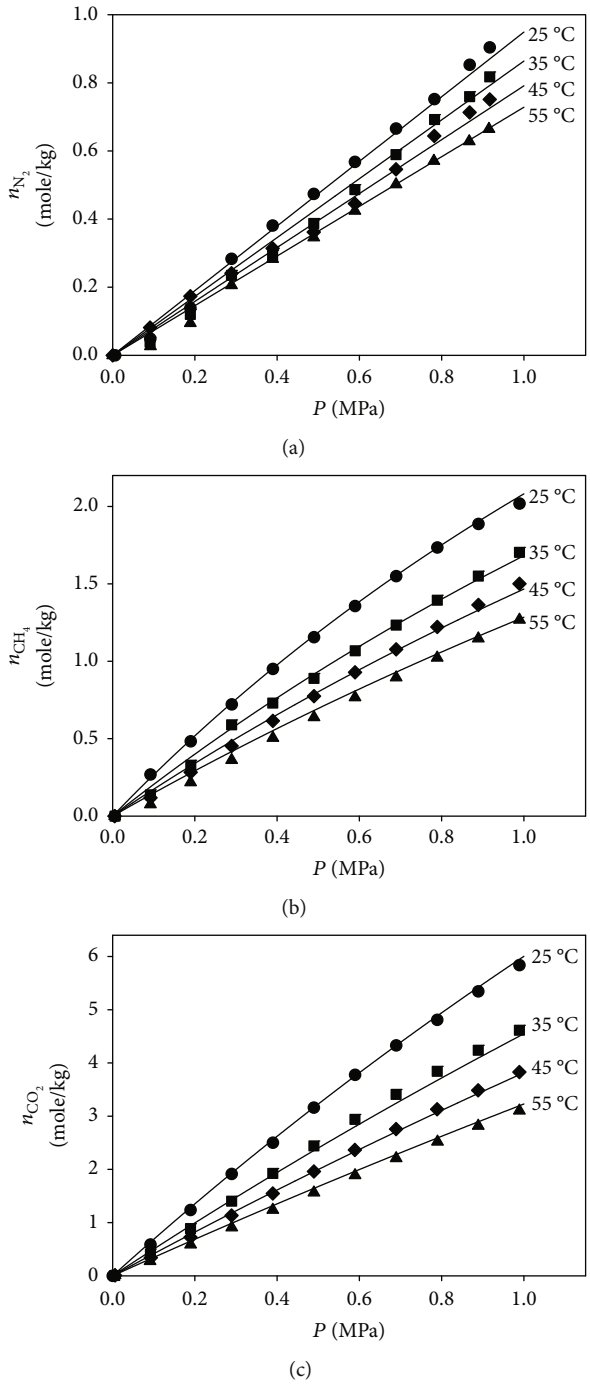

Figure 3: The adsorption equilibria of (a) nitrogen, (b) methane, and (c) carbon dioxide gases on Zn/Co-ZIF-8 at different temperatures. The symbols indicate measured results and the lines indicate DSL fitting.

equilibria of these gases were fitted perfectly, with a minor deviation, by DSL formula for the whole range of pressures and temperatures. Further, the adsorption equilibria of various gases on the ZIF-8 sample exhibited a Henry's law trend that did not seem to reach the saturation limit within the examined pressure scale. Figures 2(a)–2(c) display adsorption equilibrium isotherms of nitrogen, methane, and carbon dioxide, respectively, on Co-ZIF-8. It is observed that the DSL model has deviated slightly from experimental points of nitrogen, methane, and carbon dioxide adsorption isotherms. Figures 3(a)–3(c) show, respectively, the adsorption equilibrium of nitrogen, methane, and carbon dioxide adsorptions on Zn/Co-ZIF-8. Excellent fit of the DSL model to experimental data points is observed in the entire range of temperatures. Furthermore, Table 1 shows that for variety of the studied adsorption systems, one adsorption site was sufficient to describe the corresponding isotherm data (as exhibited by the sufficiency of $J = 1$), which reduces to the regular Langmuir adsorption isotherm and refers to an energetically homogeneous adsorbent surface towards the corresponding gas. It is noted that the results of ZIF-8 reported in Awadallah-F et al. [30] are used here for the purpose of comparison.

Figures 4(a)–4(c) illustrates the influence of various adsorbents (i.e., ZIF-8, Co-ZIF-8, and Zn/Co-ZIF-8) on the adsorption equilibria of nitrogen, methane, and carbon dioxide, respectively, at 25°C (25°C was selected as an illustration for the purpose of briefness). It is observed that the quantity adsorbed on Zn/Co-ZIF-8 is the largest in the case of N_2 and CH_4 gases, whereas ZIF-8 exhibits the biggest adsorption capacity of CO_2 gas (and the lowest adsorption capacity in the case of N_2 and CH_4 gases). Therefore, it can be said that insertion of cobalt ions into ZIF-8 leads to a noticeable change in adsorption equilibrium quantities of CH_4, N_2, and CO_2 gases.

3.2. Rate of Adsorption. Figures 5–7 illustrate the correlation between the overall mass transfer coefficient (k, sec^{-1}) of adsorbing nitrogen, methane, and carbon dioxide on ZIF-8, Co-ZIF-8, and Zn/Co-ZIF-8, correspondingly, against the reciprocal pressure ($1/P$) at different temperatures. Symbols and lines denote, correspondingly, measured data and linear regression. The regression constants were recorded in Table S1 (see Supplementary File Data). As an overview, it was noticed that k-values rise via rising temperature and via diminishing pressure (or rising reciprocal pressure). Furthermore, the k-values approach zero at extreme pressures (i.e., as $1/P \rightarrow 0$), and the influence of temperature in this case is nil. Otherwise, at mild pressures, the k-values were in the rough order of 10^{-3} s^{-1}.

Figures 5(a)–5(c) display the k-values for adsorbing nitrogen, methane, and carbon dioxide, respectively, on ZIF-8. It is noted that the adsorption of carbon dioxide on ZIF-8 is slowest, whereas the adsorption of methane is the fastest. The sequence of gas adsorption rates on ZIF-8 is $CH_4 > N_2 > CO_2$. Figures 6(a)–6(c) elucidate the k results of adsorption on Co-ZIF-8 against $1/P$. It is noted that the adsorption of nitrogen on Co-ZIF-8 is quicker than that of both carbon dioxide and methane. Moreover, the adsorption of CH_4 is faster than the adsorption of CO_2. The sequence of gas adsorption rates on Co-ZIF-8 is $N_2 > CH_4 > CO_2$. Figures 7(a)–7(c) expose that the adsorption of CH_4 on Zn/Co-ZIF-8 is the most rapid amid the gases used, whereas carbon dioxide gas was the slowest. The sequence of gas adsorption rates on Zn/Co-ZIF-8 is $CH_4 > N_2 > CO_2$.

Table 1: The fitting constants of the DSL equation for CH_4, N_2, and CO_2 on ZIF-8, Co-ZIF-8, and Zn/Co-ZIF-8.

Constants	Specimens ZIF-8			Co-ZIF-8			Zn/Co-ZIF-8		
	Gas Nitrogen	Methane	Carbon dioxide	Nitrogen	Methane	Carbon dioxide	Nitrogen	Methane	Carbon dioxide
m_1 (mole/kg)	38359	9.58	97.28	12139	7.37	21.83	13139	8.45	42.85
b_0 (MPa^{-1})	1.84×10^{-6}	9.98×10^{-4}	2.14×10^{-9}	3.91×10^{-6}	1.90×10^{-3}	1.38×10^{-5}	40.10×10^{-6}	1.17×10^{-3}	2.45×10^{-4}
ε/R (K)	693.55	1582	5038	881.97	1535.11	2917.13	861.97	1649.61	1904.60
m_2 (mole/kg)	0	0	27.89	0	0	0	0	0	0
b_0 (MPa^{-1})	0	0	7.61×10^{-2}	0	0	0	0	0	0
ε/R (K)	0	0	0	0	0	0	0	0	0
SSE	0.020	0.0082	1.07	2.04	0.13	0.22	1.52	0.11	0.22
ARE (%)	8.82	3.54	7.46	34.61	12.15	27.98	45.30	9.32	18.26

Figure 8 shows the influence of the ZIF sample type (i.e., ZIF-8, Co-ZIF-8, and Zn/Co-ZIF-8) on the k results of nitrogen, methane, and carbon dioxide gases at the temperatures of 25 and 55°C (note that these temperatures were selected as examples for the purpose of briefness). It was observed from Figures 8(a) and 8(b) that, at both temperatures, adsorbing N_2 is fastest onto the Co-ZIF-8 sample, followed by Zn/Co-ZIF-8 and then ZIF-8. Figures 8(c) and 8(d) indicate that the adsorption rate of the CH_4 gas at both temperatures followed the trend of ZIF-8 > Co-ZIF-8 > Zn/Co-ZIF-8. Additionally, it is noted from Figures 8(e) and 8(f) that the rate of CO_2 adsorption follows the order of Zn/Co-ZIF-8 > ZIF-8 > ZIF-8. It is noted that the results of ZIF-8 reported in Awadallah-F et al. [30] were used here for the purpose of comparison.

3.3. Isosteric Heat of Adsorption. Isosteric heats of adsorption (Q_{st}) were determined from the numerical differentiation of the experimental adsorption data at various temperatures in accordance to Clausius-Clapeyron's equation (Equation (3)). Figures 9(a)–9(c) expose the isosteric heats (Q_{st}) of nitrogen, methane, and carbon dioxide adsorbed on ZIF-8, Co-ZIF-8, and Zn/Co-ZIF-8, respectively. In general, it was observed that the Q_{st} of different components rises to various levels when the loading of each gas on the ZIF surface rises. This is a sign of auspicious interactions amid the molecules adsorbed to the ZIF surface [26]. The consequent trend of adsorption isosteric heats of different components (at similar gas loadings) is methane > carbon dioxide > nitrogen, which reflects their affinity for adsorption.

Nevertheless, it is noticed from Figure 9(a) that the Q_{st} of nitrogen on ZIF-8 augments from ~9 kJ/mole at a loading of 0.048 mole/kg up to ~11 kJ/mole at 0.3 mole/kg. Then, it settles at about this amount, which reveals either adsorption on a nearly nonheterogeneous surface of ZIF [26] or an equivalence between positive and negative interactions. The Q_{st} of carbon dioxide augments from ~14 kJ/mole at 0.36 mole/kg to ~33 kJ/mole at 2.81 mole/kg. Further, the Q_{st} of methane rose from ~16 kJ/mole at a loading of 0.10 mole/kg up to ~31 kJ/mole at 1.2 mole/kg.

Figure 9(b) displays that the Q_{st} of nitrogen adsorbed on Co-ZIF-8 settled at ~10 kJ/mole for loadings up to ~0.75 mole/kg. The Q_{st} of carbon dioxide gas rises from ~24 kJ/mole to ~31 kJ/mole when augmenting its loading from 0.25 to 2.56 kg/mole. Furthermore, it is seen that the Q_{st} of CH_4 rises from ~32 kJ/mole at ~0.23 mole/kg to ~41 kJ/mole at 1.40 mole/kg.

Figure 9(c) exposes that the Q_{st} of the adsorption of nitrogen on Zn/Co-ZIF-8 augments from ~8 kJ/mole up to ~11 kJ/mole when increasing the corresponding loading from 0.05 mole/kg to 0.76 mole/kg. The Q_{st} of carbon dioxide gas remains at around ~20-21 kJ/mole for the entire range of its loading. In contrast, the Q_{st} of methane rises from ~20 kJ/mole at an adsorbed amount of 0.14 mole/kg up to ~27 kJ/mole at 1.51 mole/kg.

Figures 10(a)–10(c) elucidate a disparity between the isosteric heat values of nitrogen, methane, and carbon dioxide, respectively, on various ZIFs. Overall, it was noticed from Figure 10(a) that the Q_{st} values of N_2 obeys the trend ZIF-8 > Zn/Co-ZIF-8 > Co-ZIF-8. Additionally, the Q_{st} of the adsorption of nitrogen augments with the adsorbed amount of gas on Zn/Co-ZIF-8, ZIF-8, and to a lesser extent on Co-ZIF-8. Figure 10(b) displays that the order of Q_{st} for CH_4 is Co-ZIF-8 > Zn/Co-ZIF-8 > ZIF-8 in the range from 0.15 to 0.97 mole/kg. After 0.97 mole/kg, the order of Q_{st} for CH_4 turns out to be Co-ZIF-8 > ZIF-8 > Zn/Co-ZIF-8. It is seen from Figure 10(c) that the Q_{st} value of CO_2 was always highest for Co-ZIF-8. The Q_{st} for CO_2 on Zn/Co-ZIF-8 was nearly constant at values higher than that on ZIF-8 up to a loading of 1.57 mole/kg, after which the isosteric heat on ZIF-8 becomes greater than that on Zn/Co-ZIF-8. It is noted that the results of ZIF-8 reported in Awadallah-F et al. [30] were used for the purpose of comparison.

4. Conclusions

ZIF-8, Co-ZIF-8, and Zn/Co-ZIF-8 were produced by a microwave-irradiation technique. The adsorption of CH_4, N_2, and CO_2 on ZIF-8, Co-ZIF-8, and Zn/Co-ZIF-8 was

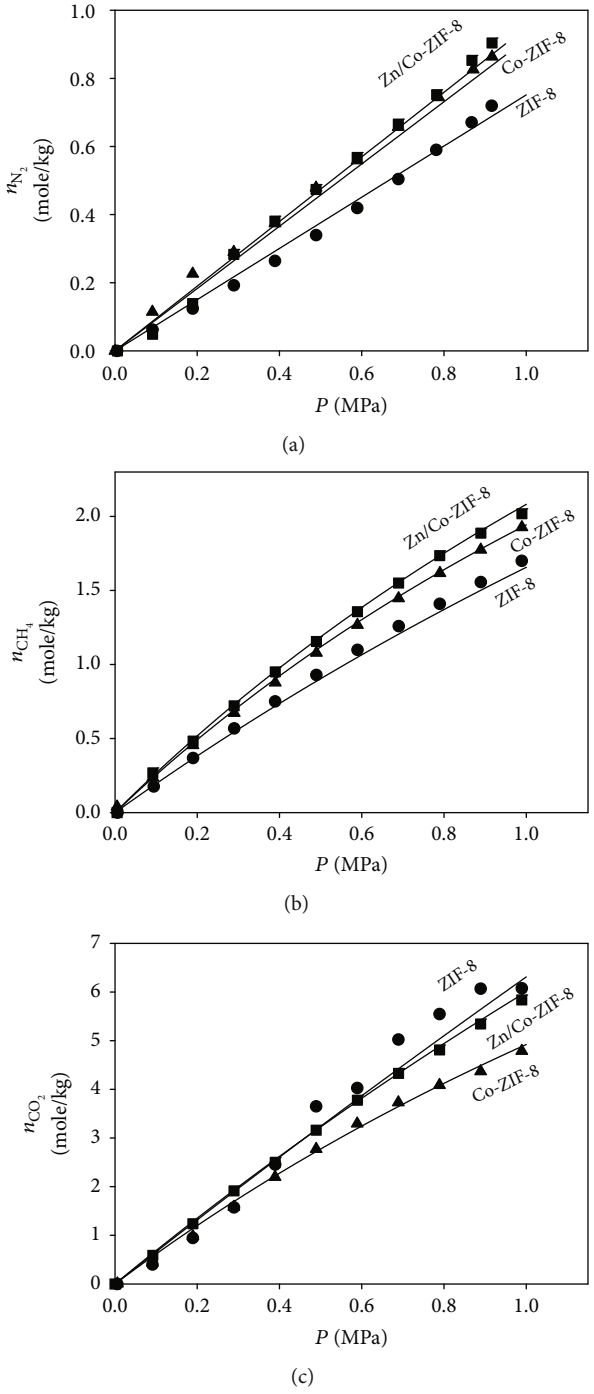

Figure 4: Influence of ZIF types (ZIF-8, Co-ZIF-8, and Zn/Co-ZIF-8) on their adsorption of (a) nitrogen, (b) methane, and (c) carbon dioxide at the temperature of 25°C. The symbols indicate measured data and the lines indicate DSL fitting.

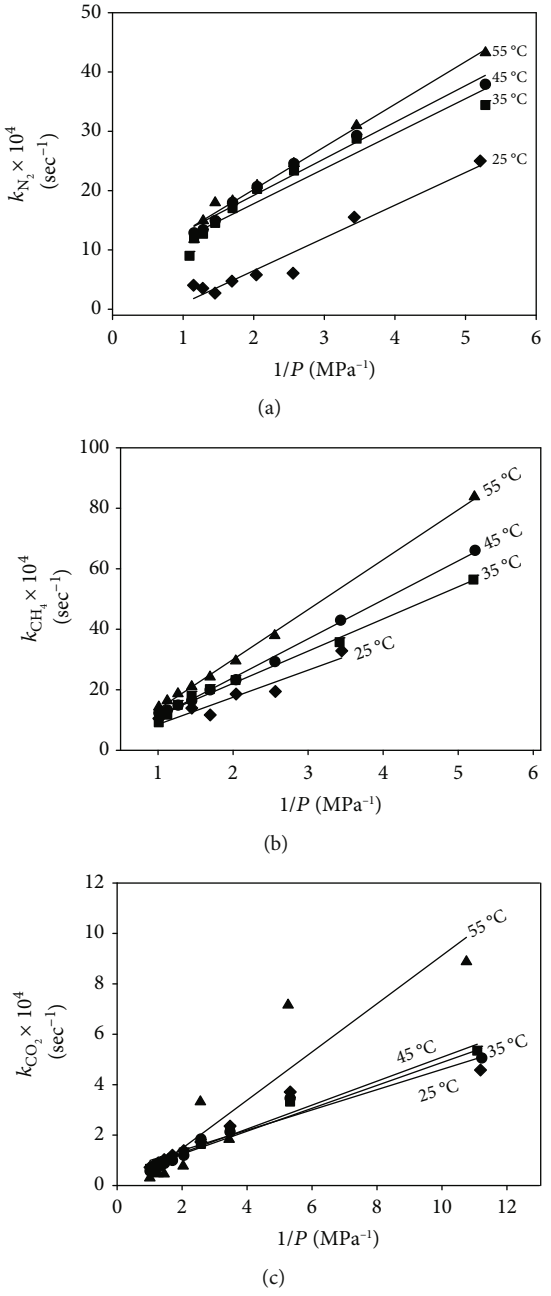

Figure 5: k-values for adsorbing (a) nitrogen, (b) methane, and (c) carbon dioxide gases on ZIF-8 samples at diverse temperatures. Symbols and lines indicate, respectively, estimated data and linear regression.

studied at a range of temperatures (25 to 55°C) and pressures (~0 to ~1 MPa). The dual-site Langmuir (DSL) model was used to describe experimental adsorption equilibria at different pressures and temperatures. Zn/Co-ZIF-8 displays the largest capacity to adsorb nitrogen and methane at various temperatures, while ZIF-8 shows the largest capacity to adsorb carbon dioxide. The order of adsorption quantities of nitrogen and methane gases on different ZIFs is Zn/Co-ZIF-8 > Co-ZIF-8 > ZIF-8. Moreover, the order of adsorption capacities of carbon dioxide gas onto different ZIFs is ZIF-8 > Zn/Co-ZIF-8 > Co-ZIF-8. The overall mass transfer coefficients have been evaluated to indicate the rates of adsorbing CH_4, N_2, and CO_2 gases on various ZIFs. Overall, the mass transfer coefficients were augmented when raising the temperature or reducing the pressure. Furthermore, the

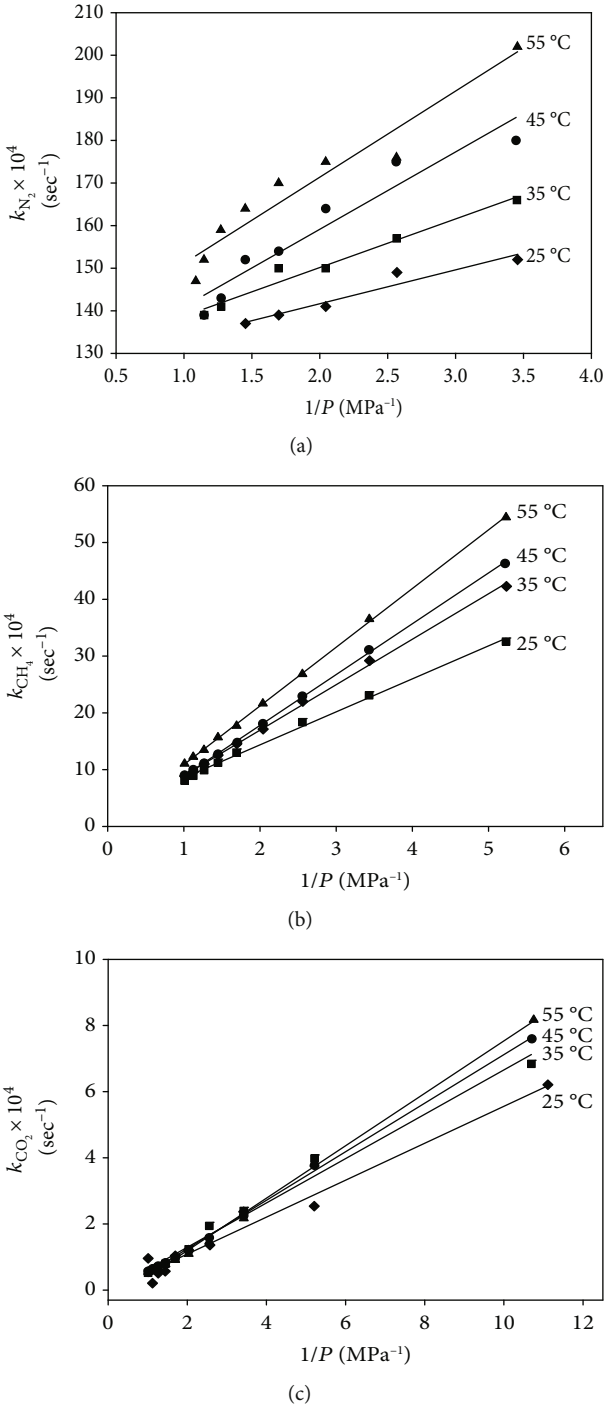

Figure 6: k-values for adsorbing (a) nitrogen, (b) methane, and (c) carbon dioxide gases on Co-ZIF-8 samples at diverse temperatures. Symbols and lines denote, respectively, estimated data and linear regression.

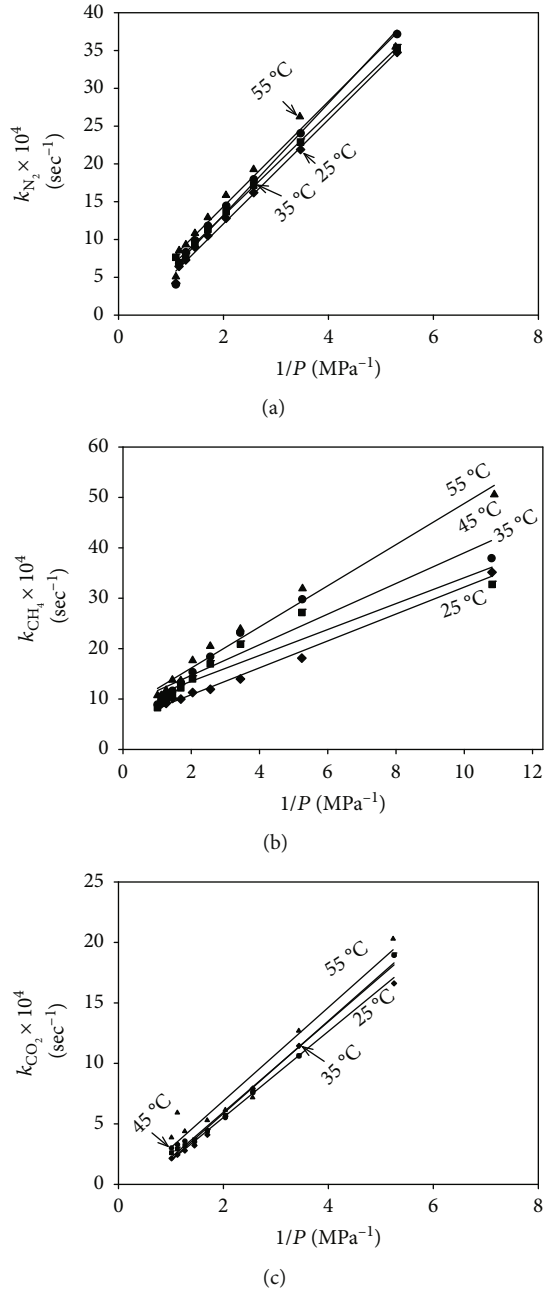

Figure 7: k-values for adsorbing (a) nitrogen, (b) methane, and (c) carbon dioxide gases on Zn/Co-ZIF-8 samples at diverse temperatures. Symbols and lines denote, respectively, estimated data and linear regression.

adsorption of CO_2 gas was slowest on all ZIFs. On the other hand, the adsorption of CH_4 gas was the fastest on ZIF-8 and Co/Zn-ZIF-8, while nitrogen adsorption was fastest on Co-ZIF-8. These disparities, which are due to the existence of cobalt into the matrix of ZIFs, can be utilized to boost the kinetic separations of CH_4, N_2, and CO_2 mixtures. Additionally, the isosteric heats of adsorbing CH_4, N_2, and CO_2 gases on ZIF-8, Co-ZIF-8, and Zn/Co-ZIF-8 were estimated. Across study findings, it has been noticed that the isosteric heats vary in accordance with the ZIF type utilized, but they were mostly highest for CH_4 and lowest for N_2.

Data Availability

The data used to support the findings of this study are included within the article.

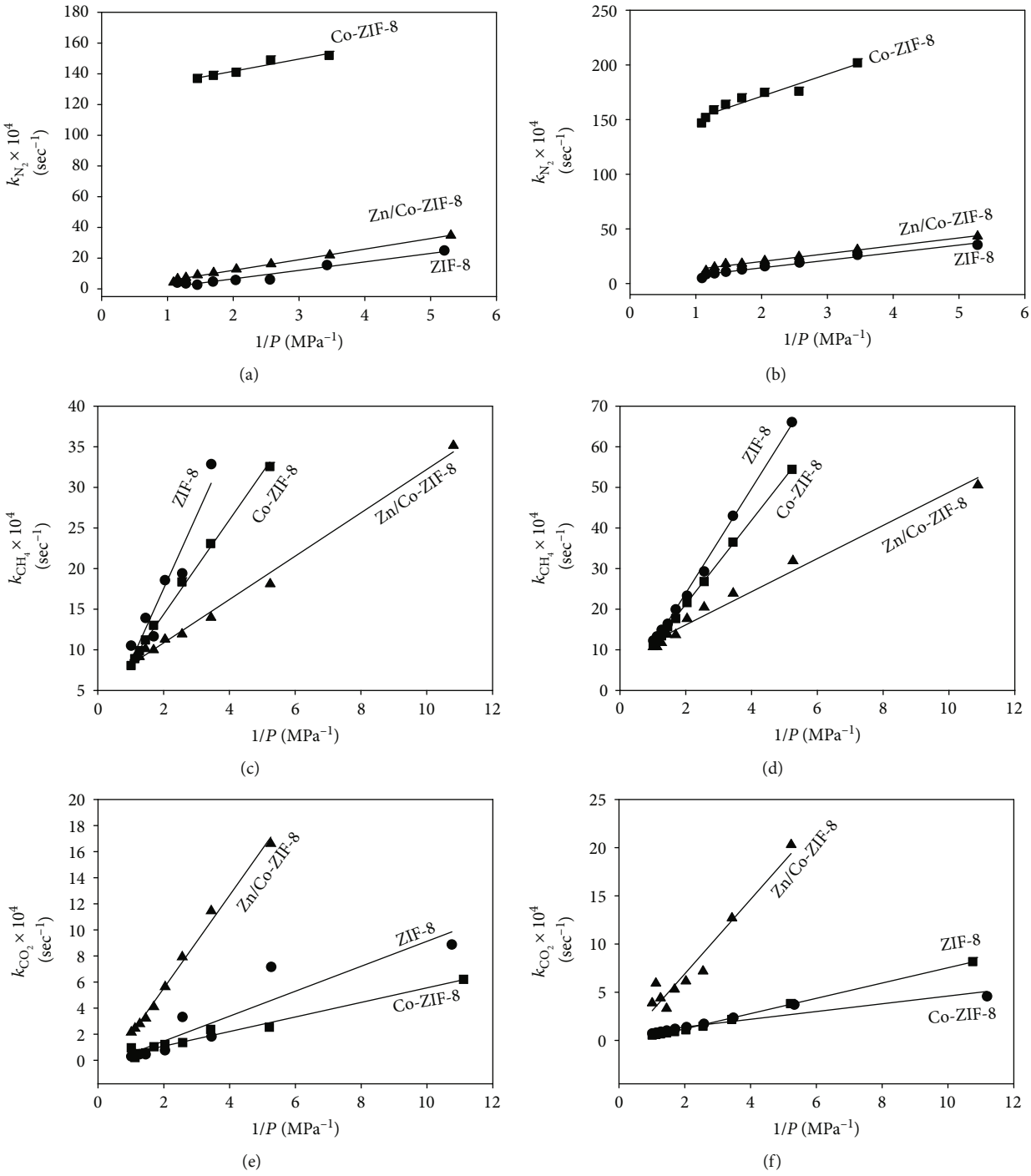

Figure 8: Impact of ZIF types (i.e., ZIF-8, Co-ZIF-8, and Zn/Co-ZIF-8) on k for (a, b) nitrogen, (c, d) methane, and (e, f) carbon dioxide at 25°C (a, c, e) and 55°C (b, d, f). Symbols and lines denote to estimated data and linear regression, correspondingly.

Disclosure

Ahmed Awadallah-F is on leave from the Radiation Research of Polymer Department, National Centre for Radiation Research and Technology, Atomic Energy Authority, P.O. Box 29, Nasr City, Cairo, Egypt. The sponsors had no role in the design, execution, interpretation, or writing of the study.

Conflicts of Interest

The authors declare no conflict of interest.

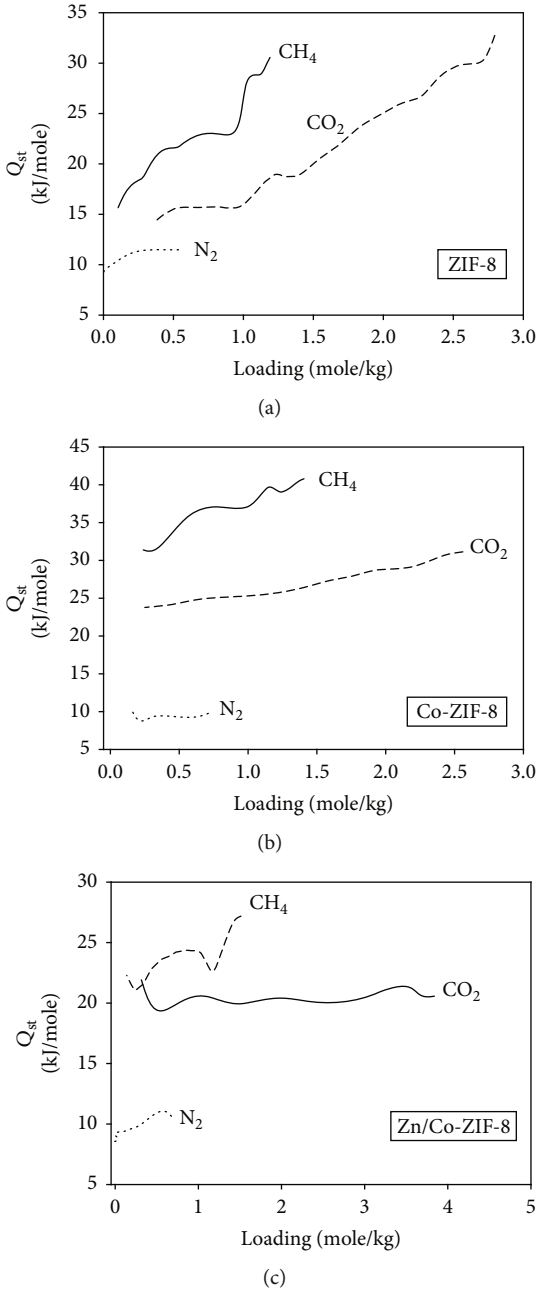

FIGURE 9: Q_{st} of adsorption of nitrogen, methane, and carbon dioxide gases upon (a) ZIF-8, (b) Co-ZIF-8, and (c) Zn/Co-ZIF-8.

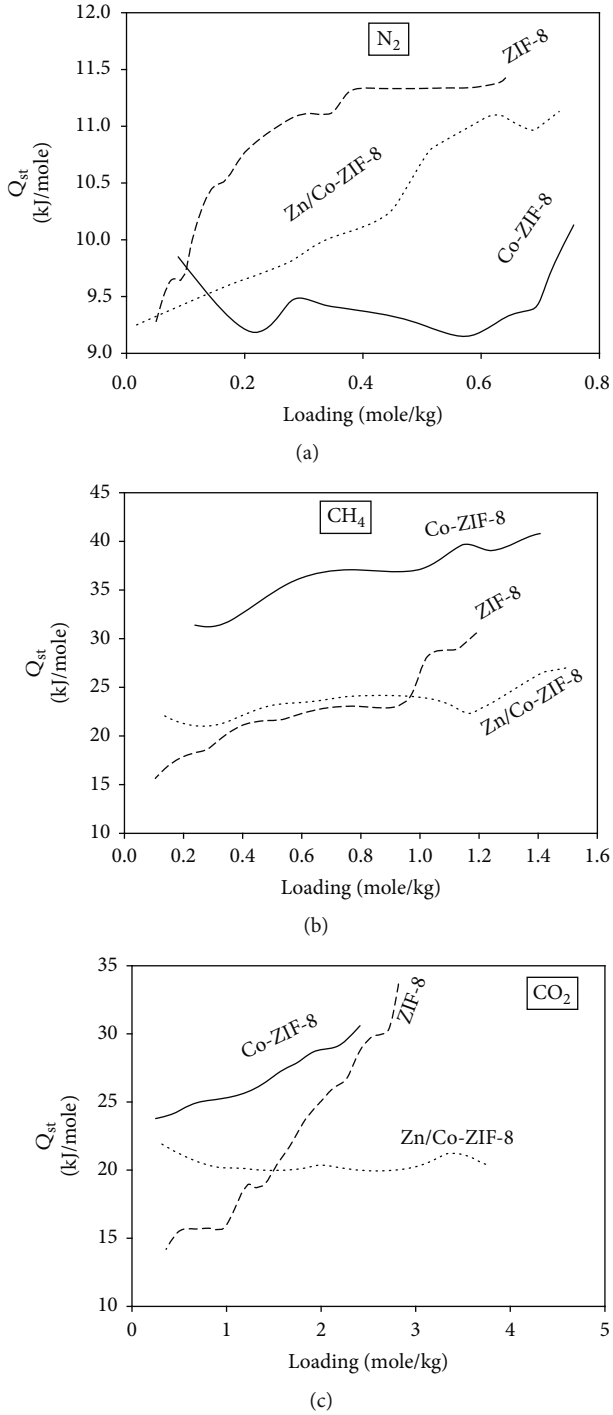

FIGURE 10: The Q_{st} of adsorption for (a) N_2, (b) CH_4, and (c) CO_2 on various ZIFs.

Acknowledgments

This publication was made possible by the NPRP awards (NPRP 08-014-2-003 and NPRP-8-001-2-001) from the Qatar National Research Fund (a member of The Qatar Foundation). H.-K.J. acknowledges support from the National Science Foundation (CMMI-1561897). The statements made herein are solely the responsibility of the authors. Technical support from the Department of Chemical Engineering, the Central Laboratory Unit (CLU), and the Gas Processing Centre (GPC) at Qatar University is also acknowledged. The publication of this article was funded by the Qatar National Library.

Supplementary Materials

S1: regression of mass transfer coefficients. Table S1 summarizes the regression of mass transfer coefficients for the adsorption of nitrogen, methane, and carbon dioxide gases onto different adsorbents of ZIFs: ZIF, Co-ZIF-8, and Zn/Co-ZIF-8. Table S1: regression and the coefficients of determination (R^2) for the overall mass transfer coefficient

$10^4 \times k$ (s^{-1}) against $1/P$ (MPa^{-1}) for adsorption of methane, nitrogen, and carbon dioxide gases on ZIF-8, Co-ZIF-8, and Zn/Co-ZIF-8 adsorbents at different temperatures. *(Supplementary Materials)*

References

[1] J. Duan, Y. Pan, G. Liu, and W. Jin, "Metal-organic framework adsorbents and membranes for separation applications," *Current Opinion in Chemical Engineering*, vol. 20, pp. 122–131, 2018.

[2] A. Awadallah-F, F. Hillman, S. A. Al-Muhtaseb, and H. K. Jeong, "Influence of doped metal center on morphology and pore structure of ZIF-8," *Material Research Society Communications*, vol. 9, no. 01, pp. 288–291, 2019.

[3] W. Li, Y. Zhang, Q. Li, and G. Zhang, "Metal–organic framework composite membranes: synthesis and separation applications," *Chemical Engineering Science*, vol. 135, pp. 232–257, 2015.

[4] L. S. Lai, Y. F. Yeong, K. K. Lau, and A. M. Shariff, "Effect of synthesis parameters on the formation of ZIF-8 under microwave-assisted solvothermal," *Procedia engineering*, vol. 148, pp. 35–42, 2016.

[5] V. V. Butova, A. P. Budnik, E. A. Bulanova, and A. V. Soldatov, "New microwave-assisted synthesis of ZIF-8," *Mendeleev Communications*, vol. 26, no. 1, pp. 43-44, 2016.

[6] A. A. Oladipo, "Microwave-assisted synthesis of high-performance polymer-based nanoadsorbents for pollution control," in *New polymer nanocomposites for environmental remediation*, C. M. Hussain and A. K. Mishra, Eds., pp. 337–359, Elsevier Inc, Amsterdam, 2018.

[7] A. Mirzaei and G. Neri, "Microwave-assisted synthesis of metal oxide nanostructures for gas sensing application: a review," *Sensors and Actuators B: Chemical*, vol. 237, pp. 749–775, 2016.

[8] H. Zhang, C. Duan, F. Li, X. Yan, and H. Xi, "Green and rapid synthesis of hierarchical porous zeolitic imidazolate frameworks for enhanced CO_2 capture," *Inorganica Chimica Acta*, vol. 482, pp. 358–363, 2018.

[9] A. Awadallah-F, F. Hillman, S. A. Al-Muhtaseb, and H.-K. Jeong, "On the nanogate-opening pressures of copper-doped zeolitic imidazolate framework ZIF-8 for the adsorption of propane, propylene, isobutane, and N-butane," *Journal of Materials Science*, vol. 54, no. 7, pp. 5513–5527, 2019.

[10] J. Peng, X. Sun, Y. Li et al., "Controllable growth of ZIF-8 layers with nanometer-level precision on SiO_2 nanopowders via liquid phase epitaxy stepwise growth approach," *Microporous and Mesoporous Materials*, vol. 268, pp. 268–275, 2018.

[11] J. H. ter Horst, C. Schmidt, and J. Ulrich, "Fundamentals of industrial crystallization," in *Handbook of Crystal Growth*, pp. 1317–1349, Bulk Crystal Growth Handbook of Crystal Growth, 2015.

[12] X. Wang, B. Yuan, X. Zhou et al., "Novel glucose-based adsorbents (Glc-Cs) with high CO_2 capacity and excellent $CO_2/CH_4/N_2$ adsorption selectivity," *Chemical Engineering Journal*, vol. 327, pp. 51–59, 2017.

[13] M. Yang, W. Jing, J. Zhao, Z. Ling, and Y. Song, "Promotion of hydrate-based CO_2 capture from flue gas by additive mixtures (THF (tetrahydrofuran) + TBAB (tetra-n-butyl ammonium bromide))," *Energy*, vol. 106, pp. 546–553, 2016.

[14] A. Dugstad, M. Halseid, and B. Morland, "Testing of CO_2 specifications with respect to corrosion and bulk phase reactions," *Energy Procedia*, vol. 63, pp. 2547–2556, 2014.

[15] K. Dalane, H. F. Svendsen, M. Hillestad, and L. Deng, "Membrane contactor for subsea natural gas dehydration: model development and sensitivity study," *Journal of Membrane Science*, vol. 556, pp. 263–276, 2018.

[16] A. Kumar and K. A. Subramanian, "Control of greenhouse gas emissions (CO_2, CH_4 and N_2O) of a biodiesel (B100) fueled automotive diesel engine using increased compression ratio," *Applied Thermal Engineering*, vol. 127, pp. 95–105, 2017.

[17] S. Rani, B. K. Prusty, and S. K. Pal, "Adsorption kinetics and diffusion modeling of CH_4 and CO_2 in Indian shales," *Fuel*, vol. 216, pp. 61–70, 2018.

[18] X. He, T. J. Kim, and M. B. Hägg, "Hybrid fixed-site-carrier membranes for CO_2 removal from high pressure natural gas: membrane optimization and process condition investigation," *Journal of Membrane Science*, vol. 470, pp. 266–274, 2014.

[19] S. K. Das, X. Wang, M. M. Ostwal, and Z. Lai, "A highly stable microporous covalent imine network adsorbent for natural gas upgrading and flue gas CO_2 capture," *Separation and Purification Technology*, vol. 170, pp. 68–77, 2016.

[20] B. Wu, X. Zhang, Y. Xu, D. Bao, and S. Zhang, "Assessment of the energy consumption of the biogas upgrading process with pressure swing adsorption using novel adsorbents," *Journal of Cleaner Production*, vol. 101, pp. 251–261, 2015.

[21] S. Yu, J. Bo, and L. Fengjuan, "Competitive adsorption of $CO_2/N_2/CH_4$ onto coal vitrinite macromolecular: effects of electrostatic interactions and oxygen functionalities," *Fuel*, vol. 235, pp. 23–38, 2019.

[22] L. Chong and E. M. Myshakin, "Molecular simulations of competitive adsorption of carbon dioxide - methane mixture on illitic clay surfaces," *Fluid Phase Equilibria*, vol. 472, pp. 185–195, 2018.

[23] F. Hillman, J. M. Zimmerman, S. M. Paek, M. R. A. Hamid, W. T. Lim, and H. K. Jeong, "Rapid microwave-assisted synthesis of hybrid zeolitic–imidazolate frameworks with mixed metals and mixed linkers," *Journal of Materials Chemistry A*, vol. 5, no. 13, pp. 6090–6099, 2017.

[24] A. Awadallah-F, S. A. al-Muhtaseb, and H. K. Jeong, "Selective adsorption of carbon dioxide, methane and nitrogen using resorcinol-formaldehyde-xerogel activated carbon," *Adsorption*, vol. 23, no. 7-8, pp. 933–944, 2017.

[25] A. Awadallah-F and S. A. Al-Muhtaseb, "Carbon dioxide sequestration and methane removal from exhaust gases using resorcinol–formaldehyde activated carbon xerogel," *Adsorption*, vol. 19, no. 5, pp. 967–977, 2013.

[26] H. Li, J. Kang, F. Zhou, Z. Qiang, and G. Li, "Adsorption heat features of coalbed methane based on microcalorimeter," *Journal of Loss Prevention in the Process Industries*, vol. 55, pp. 437–449, 2018.

[27] D. Leinekugel-le-Cocq, M. Tayakout-Fayolle, Y. Le Gorrec, and C. Jallut, "A double linear driving force approximation for non-isothermal mass transfer modeling through bi-

disperse adsorbents," *Chemical Engineering Science*, vol. 62, no. 15, pp. 4040–4053, 2007.

[28] M. Li and X. Liu, "The least squares based iterative algorithms for parameter estimation of a bilinear system with autoregressive noise using the data filtering technique," *Signal Process*, vol. 147, pp. 23–34, 2018.

[29] V. S. Mane and P. V. V. Babu, "Studies on the adsorption of brilliant green dye from aqueous solution onto low-cost NaOH treated saw dust," *Desalination*, vol. 273, no. 2-3, pp. 321–329, 2011.

[30] A. Awadallah-F, F. Hillman, S. A. al-Muhtaseb, and H. K. Jeong, "Adsorption equilibrium and kinetics of nitrogen, methane and carbon dioxide gases onto ZIF-8, Cu10%/ZIF-8, and Cu30%/ZIF-8," *Industrial & Engineering Chemistry Research*, vol. 58, no. 16, pp. 6653–6661, 2019.